Supplementary Information

Single-Molecule Magnet Behavior for an Antiferromagnetically Superexchange-Coupled Dinuclear Dysprosium(III) Complex.

Jérôme Long,[a,b] Fatemah Habib,[a,b] Po-Heng Lin,[a,b] Ilia Korobkov,[a] Gary Enright,[c] Liviu Ungur,[d] Wolfgang Wernsdorfer,[e] Liviu F. Chibotaru,[d] Muralee Murugesu*[a,b]

[a] *Department of Chemistry, University of Ottawa, 10 Marie-Curie, Ottawa, ON, K1N6N5, Canada.*

[b] *Centre for Catalysis Research and Innovation, 30 Marie-Curie, Ottawa, ON, K1N6N5, Canada.*

[c] *Steacie Institute for Molecular Sciences, NRC, 100 Sussex Drive, Ottawa, ON, K1A0R6, Canada.*

[d] *Division of Quantum and Physical Chemistry and INPAC—Institute for Nanoscale Physics and Chemistry, Katholieke Universiteit Leuven, Celestijnenlaan, 200F, 3001, Belgium.*

[e] *Institut Néel, CNRS & Université J. Fourier, BP 166 25, Avenue des Martyrs, 38042, Grenoble, France.*

Experimental

Infra Red and Elemental Analysis data.

1 (KBr, cm^{-1}): 3426(br), 3214(m), 2919(w), 2847(w), 1634(s), 1616(s), 1549(w), 1469(s), 1450(s), 1401(m), 1383(s), 1322(m), 1290(m) 1260(m), 1241(s), 1220(m), 1162(w), 1111(w), 1087(m), 1050(w), 972(m), 847(w), 740(s). Anal. Calcd for $C_{40}H_{46}Eu_2N_8O_{14}$: C, 41.18; H, 3.97; N, 9.60. Found: C, 40.05; H, 3.77; N, 9.46.

2: 3421(br), 3214(m), 2919(w), 2847(w), 1634(s), 1616(s), 1548(m), 1498(s), 1464(s), 1447(s), 1401(m), 1381(s), 1850(w), 1822(m), 1289(m), 1260(m), 1240(s), 1220(m), 1165(w), 1111(w), 1080(m), 1029(w), 997(w), 974(m), 918(w), 850(w), 741(s). Anal. Calcd for $C_{40}H_{46}Gd_2N_8O_{14}$: C, 40.81; H, 3.94; N, 9.52. Found: C, 40.72; H, 4.00; N, 9.58

3: 3421(br), 3219(m), 2919(w), 2852(w), 1636(s), 1619(s), 1550(m), 1492(s), 1467(s), 1450(s), 1402(m), 1382(s), 1350(w), 1326(m), 1292(m), 1262(m), 1239(s), 1223(m), 1165(w), 1111(w), 1080(m), 1029(w), 997(w), 971(m), 921(w), 850(w), 742(s). Anal. Calcd for $C_{40}H_{46}Tb_2N_8O_{14}$: C, 40.69; H, 3.93; N, 9.49. Found: C, 40.33; H, 3.89; N, 9.62.

4: 3225(br), 3215(m), 2918(w), 2850(w), 1637(s), 1622(s), 1551(m), 1491(s), 1469(s), 1453(s), 1401(m), 1351(w), 1325(m), 1295(m), 1262(m), 1236(s), 1225(s), 1160(w), 1111(w), 1082(m), 1027(w), 1000(w), 971(m), 920(w), 846(w), 740(s). Anal. Calcd for $C_{40}H_{46}Dy_2N_8O_{14}$: C, 40.45; H, 3.90; N, 9.43. Found: C, 40.56; H, 4.40; N, 9.39.

5: 3431(br), 3219(m), 2919(w), 2847(w), 1635(s), 1620(s), 1548(m), 1492(s), 1467(s), 1451(s), 1399(m), 1384(s), 1352(w), 1324(m), 1295(m), 1257(m), 1237(s), 1222(m), 1162(w), 1110(w), 1086(m), 1029(w), 997(w), 971(m), 921(w), 847(w), 741(s). Anal. Calcd for $C_{40}H_{46}Ho_2N_8O_{14}$: C, 40.28; H, 3.89; N, 9.39. Found: C, 40.60; H, 3.81; N, 9.25.

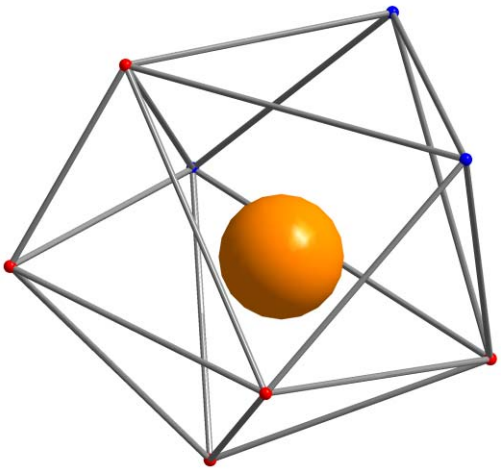

Figure S1: The coordination polyhedra of the octacoordinated Dy^{III} ion.

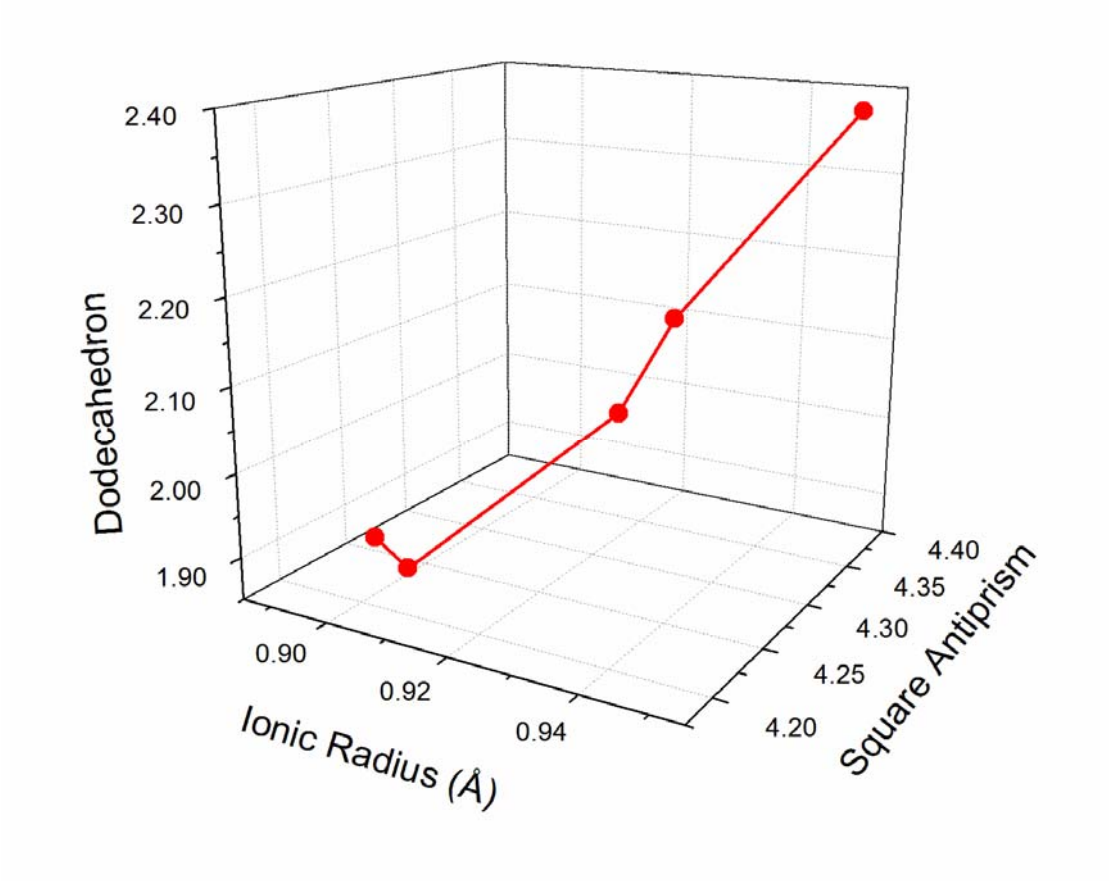

Figure S2: Plot of the *SHAPE* results as a function of ionic radius.

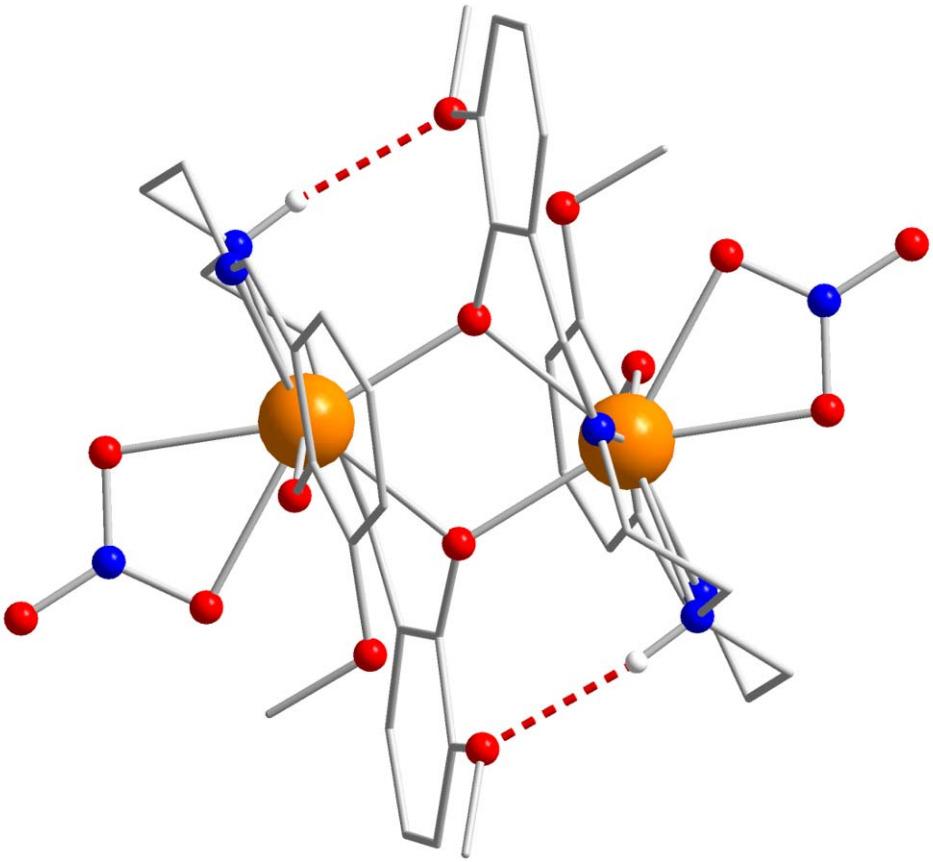

Figure S3: Intramolecular H-bond (red dashed line) in **4**.

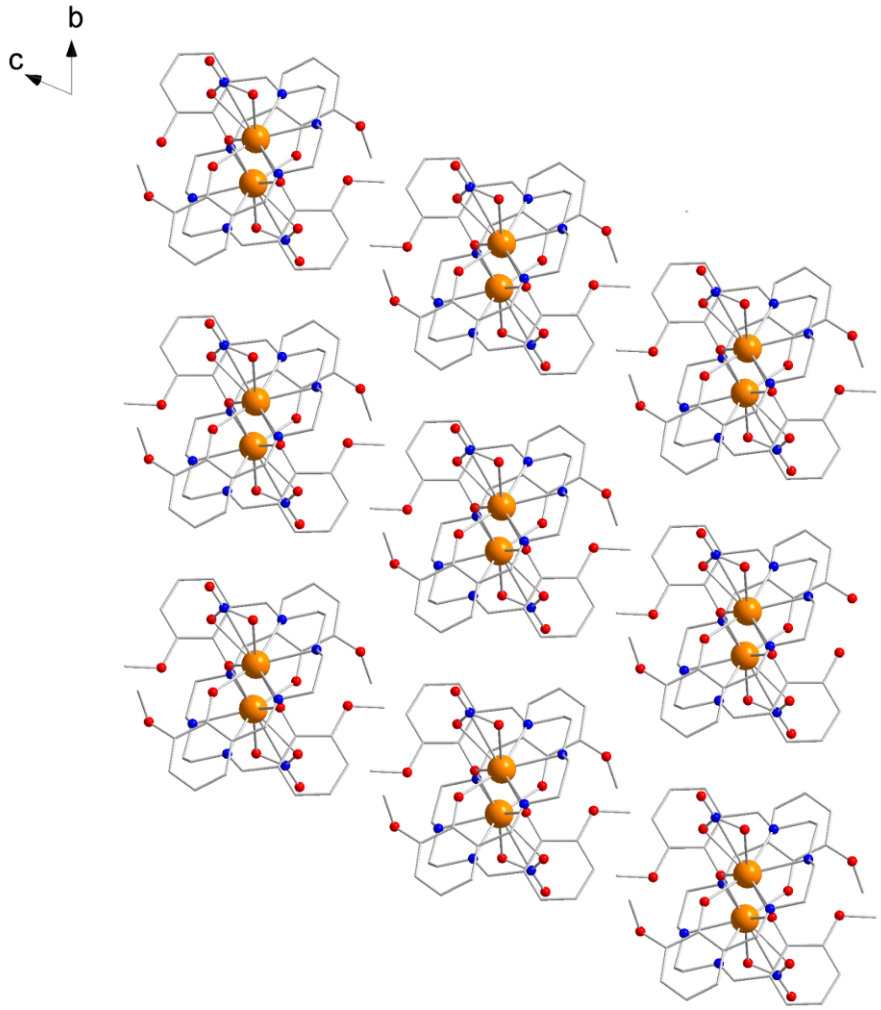

Figure S4: View of the packing arrangement along the crystallographic *a*-axis for **4**.

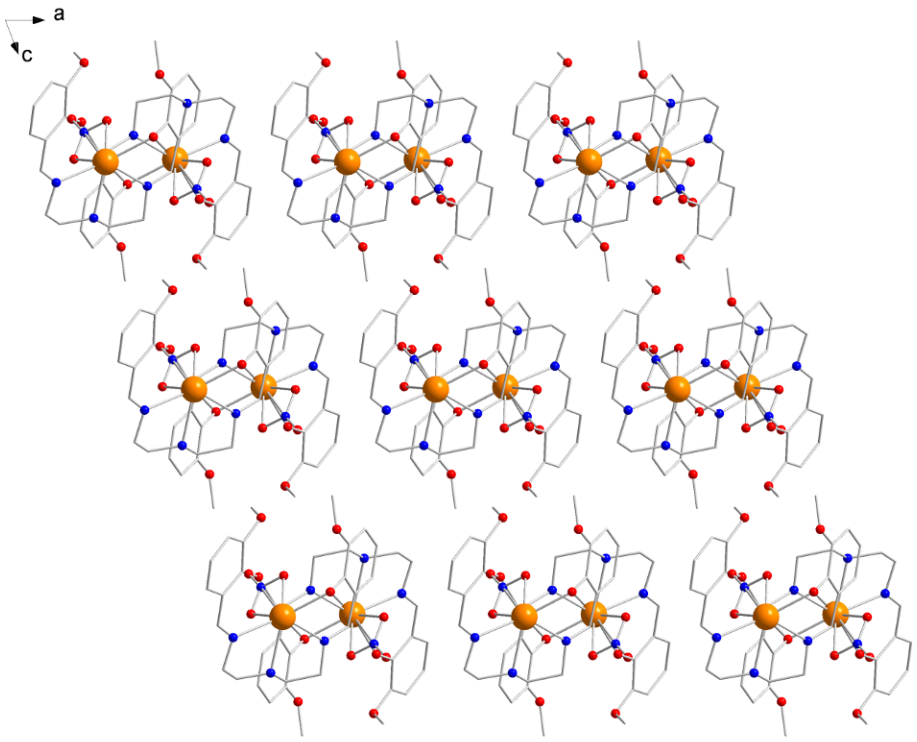

Figure S5: View of the packing arrangement along the crystallographic *b*-axis for **4**.

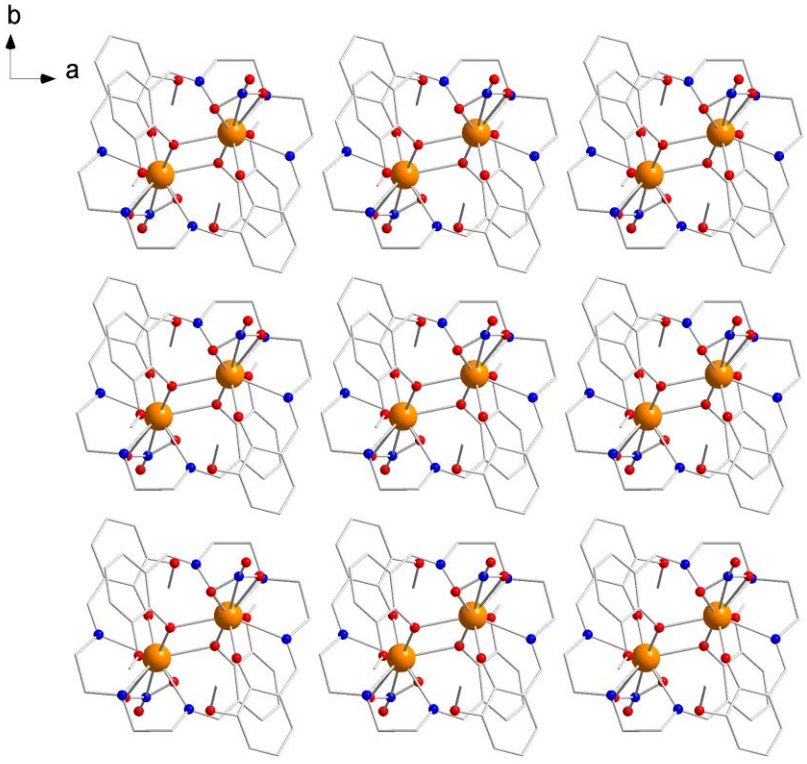

Figure S6: View of the packing arrangement along the crystallographic *c*-axis for **4**.

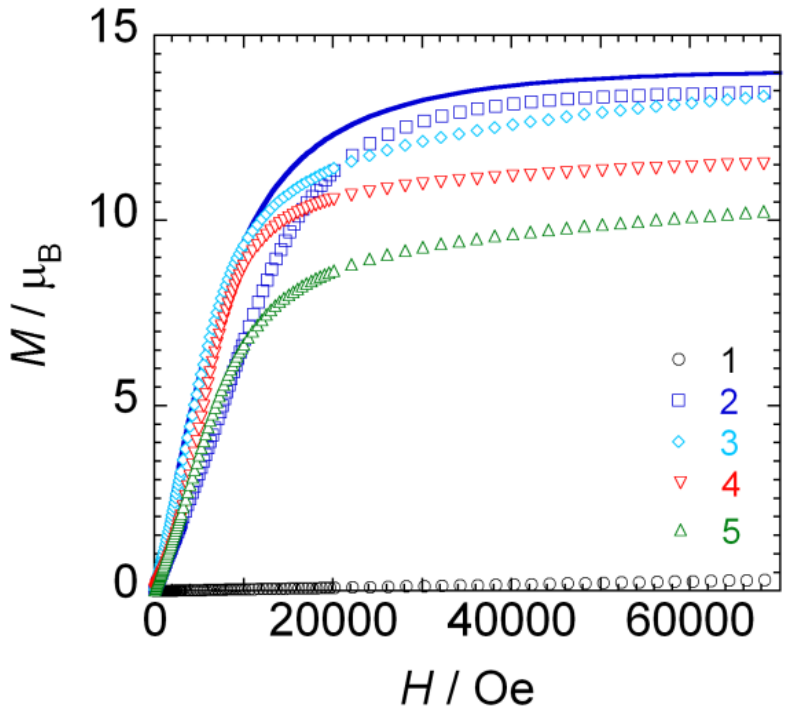

Figure S7: Field dependence of the magnetization, *M*, at 1.8 K for compounds **1 – 5**. Solid line corresponds to the Brillouin function for two uncoupled $S = 7/2$ (see Figures S4-S8 for reduced magnetization plots of **1**-**5**).

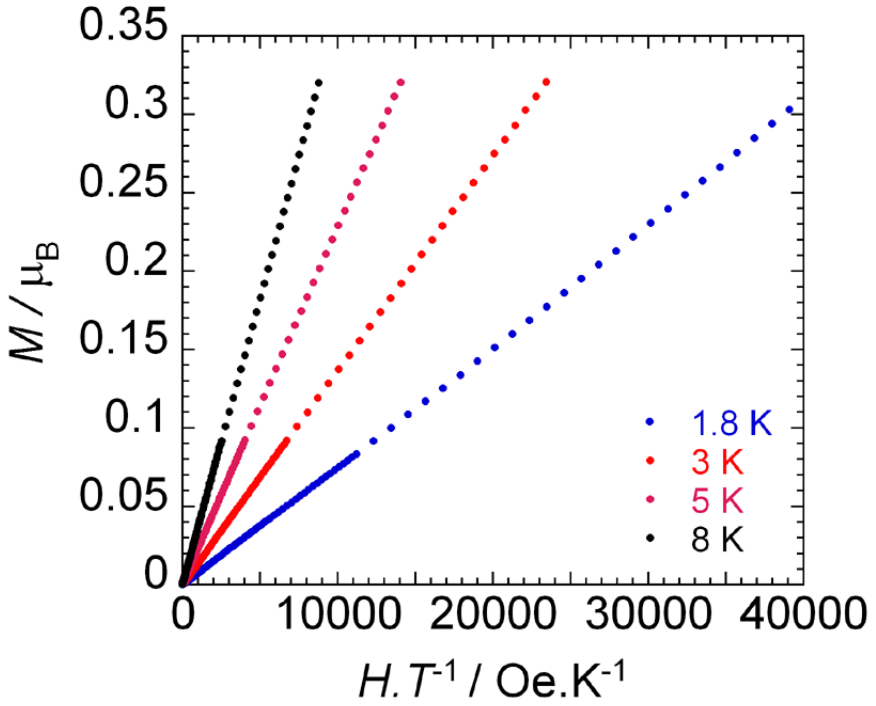

Figure S8: Field dependence of the magnetization between 1.8 and 8 K for **1**.

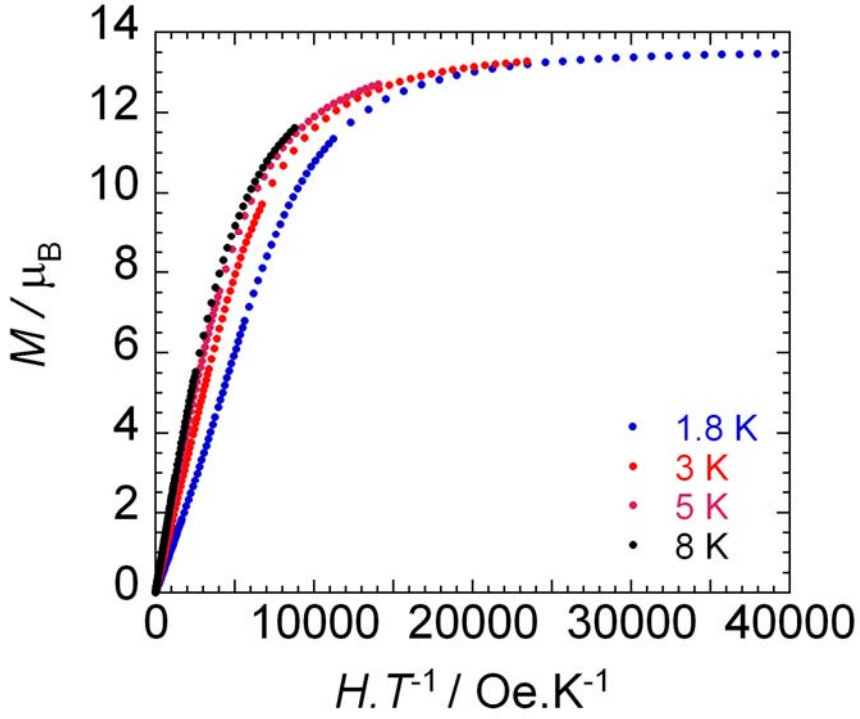

Figure S9: Field dependence of the magnetization between 1.8 and 8 K for **2**.

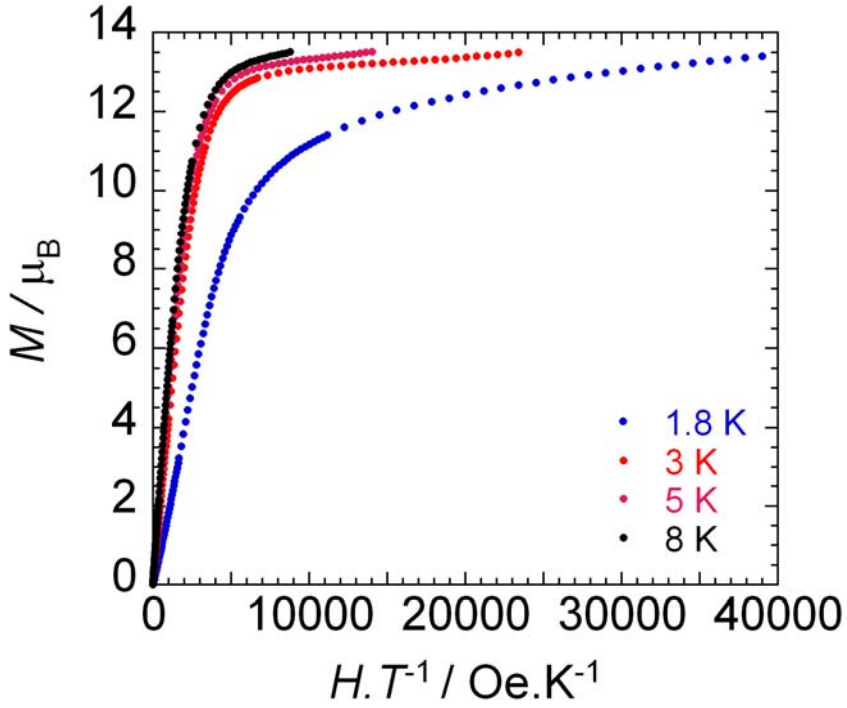

Figure S10: Field dependence of the magnetization between 1.8 and 8 K for **3**.

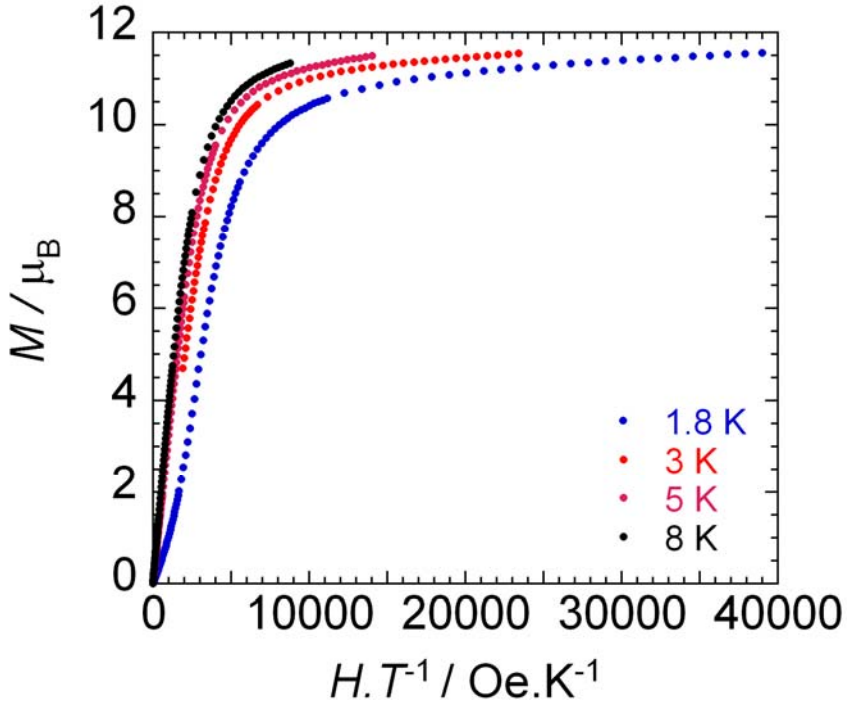

Figure S11: Field dependence of the magnetization between 1.8 and 8 K for **4.**

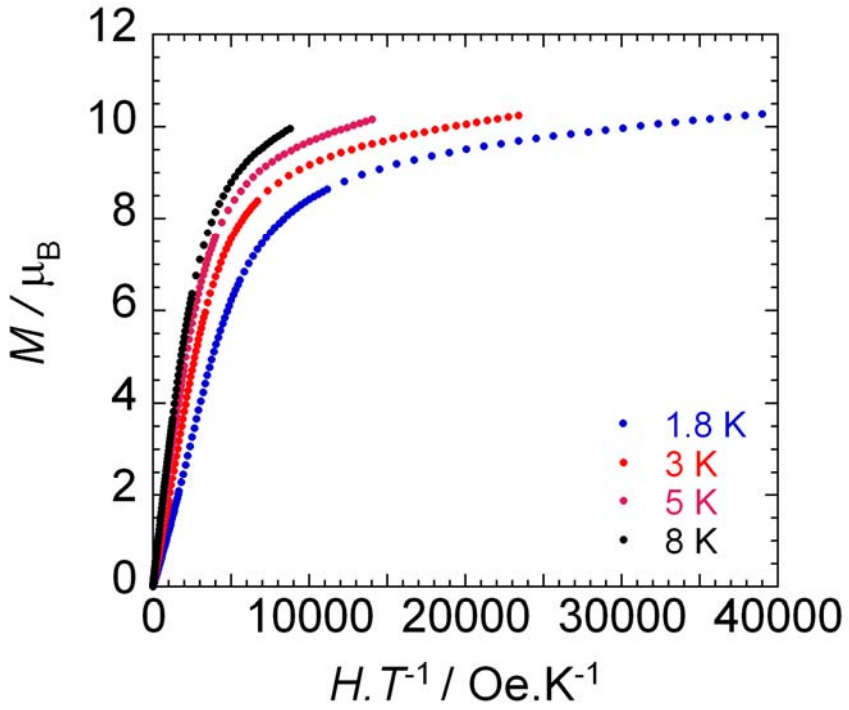

Figure S12: Field dependence of the magnetization between 1.8 and 8 K for **5**.

***Ab initio* results of the fragment calculation of Eu_2 complex (1).**

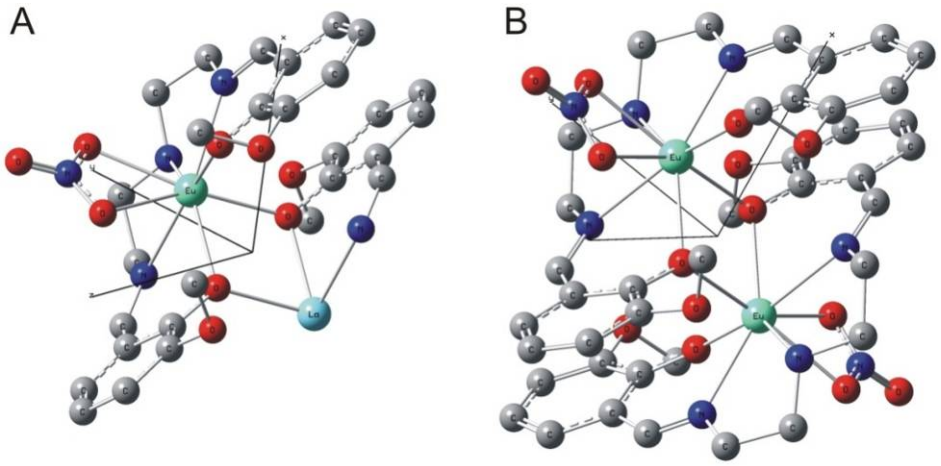

Figure S13: Calculated Eu^{III} fragment. In both fragments, the neighboring Eu^{III} was computationally simulated by non-magnetic La^{III}.

Basis Sets

ANO-RCC [8s7p5d4f2g1h] – for Eu^{III}.
ANO-RCC [4s3p2d] – for close O and N.
ANO-RCC [3s2p] – for distant O and N, and all C.
ANO-RCC [2s] – for H.
ECP---La.ECP.deGraaf.0s.0s.0e-La($LaMnO_3$). – for neighboring Eu^{III} in A.
La.ECP.Casarrubios.13s10p8d.3s3p3d.9e-CG-AIMP. – for neighboring Eu^{III} in B.

Table S1: Calculated energies of the spin-orbit states of Eu^{III} fragment.

	Fragment A			Fragment B		
	1	**2**	**3**	**1**	**2**	**3**
1	0.000	0.000	0.000	0.000	0.000	0.000
2	101.860	208.547	231.432	123.865	235.951	259.453
3	273.267	378.847	401.711	253.485	363.011	386.403
4	429.725	531.867	554.371	392.548	496.043	519.045
5	628.622	899.761	941.396	609.591	892.768	935.722
6	676.208	960.062	1002.795	668.057	965.083	1008.903
7	802.393	1078.854	1121.218	758.467	1044.324	1087.713
8	859.612	1139.114	1181.665	829.640	1117.520	1161.153
9	874.699	1156.185	1199.146	847.842	1137.102	1180.750
10	1392.231	1856.677	1905.155	1377.045	1849.928	1899.243

1: spin – free states coming from ^7F multiplet were mixed by spin–orbit coupling.
2: states coming from ^7F, ^5D, ^5L, ^5G, ^5H, ^5I, ^5F, ^5K, ^5G and ^5D multiplets were mixed by spin–orbit coupling.
3 : states coming from ^7F, ^5D, ^5L, ^5G, ^5H, ^5I, ^5F, ^5K, ^5G, ^5D, ^3P, ^3O, ^3M, ^3K, ^3H, ^3F, ^3I and ^1Q multiplets were mixed by spin–orbit coupling.

***Ab initio* results of the fragment calculation of Gd_2 complex (2).**

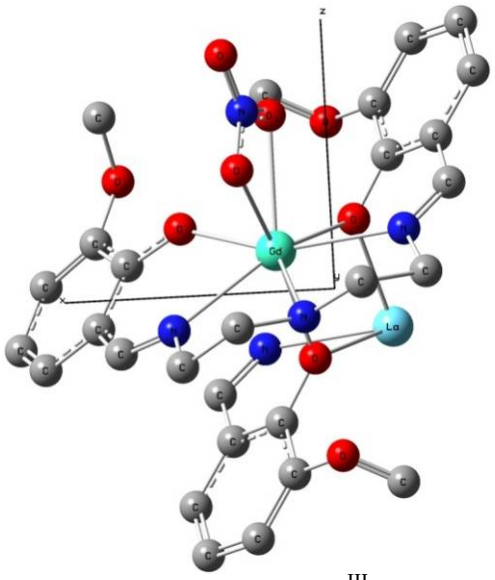

Figure S14: Calculated Gd^{III} fragment.

Basis Sets

ANO-RCC [8s7p5d4f2g1h] – for Gd^{III}.
ANO-RCC [4s3p2d] – for close O and N.
ANO-RCC [3s2p] – for distant O and N, and all C.
ANO-RCC [2s] – for H.
ECP---La.ECP.deGraaf.0s.0s.0e-La($LaMnO_3$). – for neighboring Gd^{III}.

Table S2: Calculated energies of the spin-free states (SFS) of Gd^{III} fragment.

	1	**2**
1	0.000	0.000
2	0.263	0.278
3	0.587	0.616
4	1.091	1.152
5	40589.483	39568.319
6	40618.479	39614.691
7	40669.496	39653.447
8	41124.727	39713.398
9	41171.019	40037.100
10	41252.488	40064.665

1: states coming from ^8S, ^6P, ^6I, ^6D, ^6G, ^6F, ^6H multiplets were mixed by spin–orbit coupling.
2: states coming from ^8S, ^6P, ^6I, ^6D, ^6G, ^6F, ^6H, ^4D, ^4N, ^4H, ^4L, ^4K, ^4F, ^4F, ^4G, ^4H, ^4G, ^4S, ^4I, ^4I, ^4D, ^4M, ^4K multiplets were mixed by spin–orbit coupling.

***Ab initio* results of the fragment calculation of Tb_2 complex (3).**

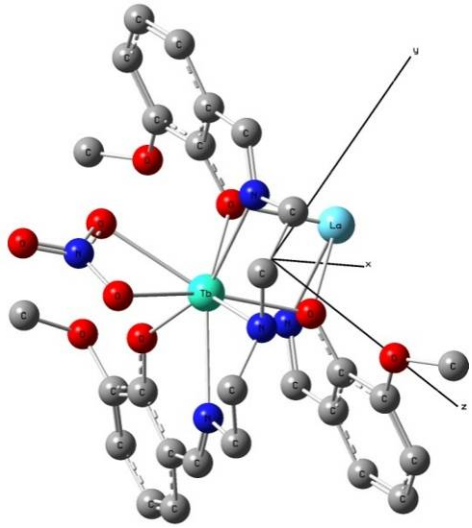

Figure S15: Calculated Tb^{III} fragment.

Basis Sets

ANO-RCC [8s7p5d4f2g1h] – for Tb^{III}.
ANO-RCC [4s3p2d] – for close O and N.
ANO-RCC [3s2p] – for distant O and N, and all C.
ANO-RCC [2s] – for H.
ECP---La.ECP.deGraaf.0s.0s.0e-La($LaMnO_3$). – for neighboring Tb^{III}.

Table S3: Calculated energies of the spin-orbit states of Tb^{III} fragment.

	1	**2**	**3**
1	0.000	0.000	0.000
2	1.213	1.226	1.229
3	44.290	43.154	43.059
4	45.789	44.653	44.560
5	71.292	71.568	71.631
6	76.029	76.126	76.163
7	138.365	139.472	139.577
8	164.753	165.902	165.990
9	217.444	217.413	217.426
10	225.779	229.671	229.994
11	255.169	257.118	257.292
12	536.850	533.034	532.957
13	538.324	534.238	534.142
14	1774.044	2049.941	2071.868
15	1778.857	2054.641	2076.578
16	1897.399	2171.086	2193.097
17	1909.141	2182.756	2204.677
18	1938.132	2211.823	2233.767
19	1968.431	2243.153	2265.341
20	2033.393	2302.922	2324.640

1: spin – free states coming from ^7F multiplet were mixed by spin–orbit coupling.
2: states coming from ^7F, ^5D, ^5L, ^5G, ^5H, ^5I, ^5F, ^5K, ^5G and ^5D multiplets were mixed by spin–orbit coupling.
3: states coming from ^7F, ^5D, ^5L, ^5G, ^5H, ^5I, ^5F, ^5K, ^5G, ^5D, ^3P, ^3O, ^3M, ^3K, ^3H, ^3F, ^3I and ^1Q multiplets were mixed by spin–orbit coupling.

***Ab initio* results of the fragment calculation of Dy_2 complex (4).**

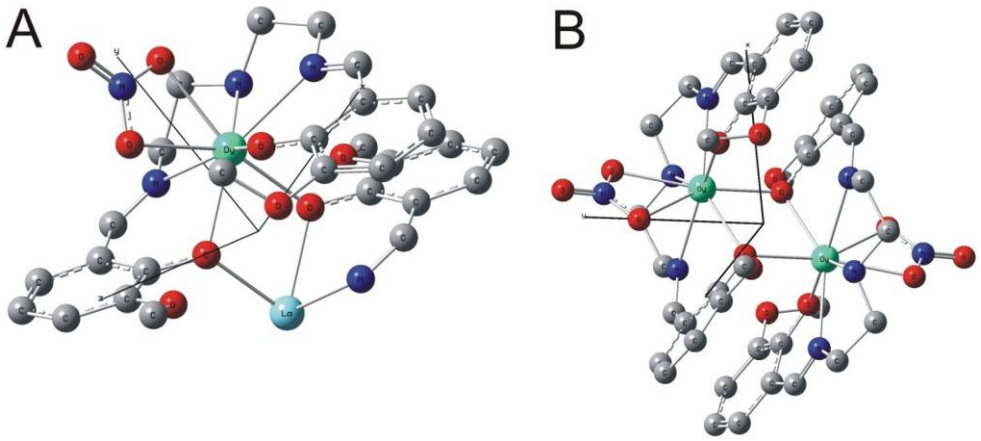

Figure S16: Calculated Dy^{III} fragments.

In the largest computational approximation (**5**) the whole molecule was kept as is. The only change was the substitution of the neighboring Dy^{III} ion with diamagnetic La^{III}.

Basis Sets were of ANO-RCC type with the following contractions.

Basis Set	**1**	**2**	**3**	**4**	**5**
Dy^{III}	7s6p4d3f1g	7s6p4d3f1g	8s7p5d4f2g1h	8s7p5d4f2g1h	8s7p5d4f2g1h
O*	3s2p1d	3s2p1d	4s3p2d1f	4s3p2d1f	4s3p2d
N*	3s2p1d	3s2p1d	4s3p2d1f	4s3p2d1f	4s3p2d
O	-	-	3s2p	3s2p	3s2p
N	3s2p	3s2p	3s2p	3s2p	3s2p
C	3s2p	3s2p	3s2p	3s2p	3s2p
H	2s	2s	2s	2s	2s

*- atoms from the first coordination sphere

Modeling of the neighboring Dy^{III} ion in our computational approximations:

1	La.ECP.deGraaf.0s.0s.0e-La($LaMnO_3$)
2	-
3	-
4	La.ECP.Casarrubios.13s10p8d.3s3p3d.9e-CG-AIMP
5	La.ECP.Casarrubios.13s10p8d.3s3p3d.9e-CG-AIMP

Table S4: Energies of the lowest Kramers doublets of the Dy^{III} fragments, and the *g*-tensor of the ground Kramers doublet in all computational approximations.

Computational approximation	**1**	**2**	**3**	**4**	**5**
Fragment	**A**	**A**	**A**	**A**	**B**
Energies (cm^{-1})	0.000	0.000	0.000	0.000	0.000
	201.707	62.164	58.386	231.266	164.445
	284.148	118.061	112.483	368.382	254.694
	369.915	205.130	177.888	427.038	293.732
	473.109	256.849	244.457	523.149	338.362
	558.115	317.602	303.248	599.951	390.460
	601.946	416.659	394.038	634.549	455.609
	654.743	524.107	498.132	688.883	516.889
	3664.045	3622.976	3618.877	3674.094	3608.162
g-tensor of the first Kramers Doublet	*g*x = 0.0095	*g*x = 0.404	*g*x = 0.385	*g*x = 0.0037	*g*x = 0.0074
	*g*y = 0.020	*g*y = 1.420	*g*y = 1.332	*g*y = 0.0080	*g*y = 0.0158
	*g*z = 19.645	*g*z = 18.036	*g*z = 18.069	*g*z = 19.713	*g*z = 19.547
Angle of the main magnetic axis with the shortest Dy-O bond (2.19 Å) (in degrees)	3.9	11.9	13.4	3.96	4.05

***Ab initio* results of the fragment calculation of Ho_2 complex (5).**

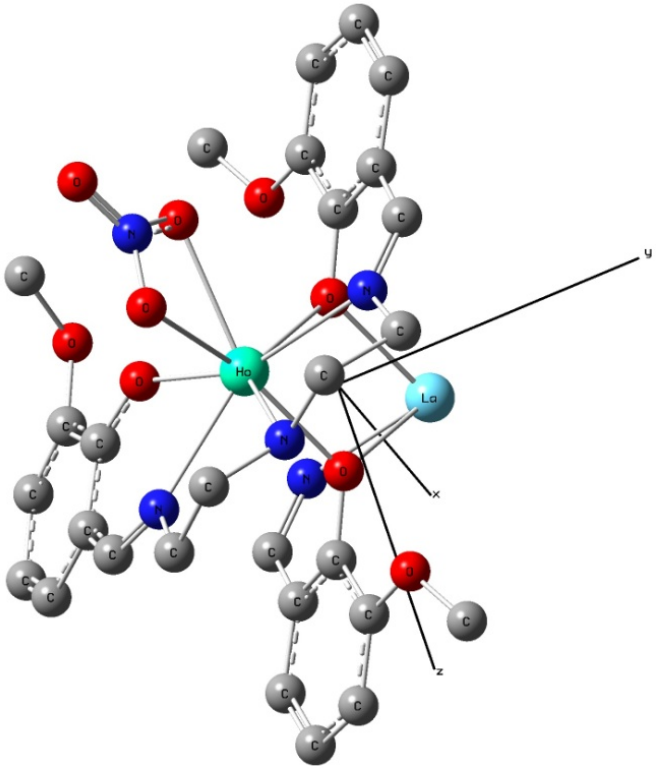

Figure S17: Calculated Ho^{III} fragment.

Basis Sets

ANO-RCC [8s7p5d4f2g1h] – for Ho^{III}.

ANO-RCC [4s3p2d] – for close O and N.

ANO-RCC [3s2p] – for distant O and N, and all C.

ANO-RCC [2s] – for H.

ECP---La.ECP.deGraaf.0s.0s.0e-La($LaMnO_3$). – for neighboring Ho^{III}.

Table S5: Calculated energies of the spin-orbit states of Ho^{III} fragment .

	1	**2**
1	0.000	0.000
2	1.567	1.457
3	70.504	66.987
4	77.881	73.799
5	132.847	125.780
6	140.500	132.766
7	198.300	186.895
8	200.628	189.037
9	245.565	231.991
10	248.577	234.947
11	279.680	265.173
12	292.786	277.275
13	308.725	292.009
14	313.290	296.349
15	337.588	319.263
16	345.232	326.207
17	355.412	335.886
18	4476.591	5183.279
19	4476.866	5183.533
20	4546.273	5251.065

1: states coming from ^{5}I, ^{5}S, ^{5}F, ^{5}G, ^{5}D multiplets were mixed by spin–orbit coupling.

2: states coming from ^{5}I, ^{5}S, ^{5}F, ^{5}G, ^{5}D, ^{3}K, ^{3}H, ^{3}G, ^{3}L, ^{3}D, ^{3}P, ^{3}M, ^{3}F, ^{3}I, ^{3}F, ^{3}H, ^{3}G, ^{3}F, ^{3}K, ^{3}H, ^{1}L, ^{1}D, ^{1}G, ^{1}I, ^{1}H, ^{1}K, ^{1}D, ^{1}M, ^{1}G, ^{1}L multiplets were mixed by spin–orbit coupling.

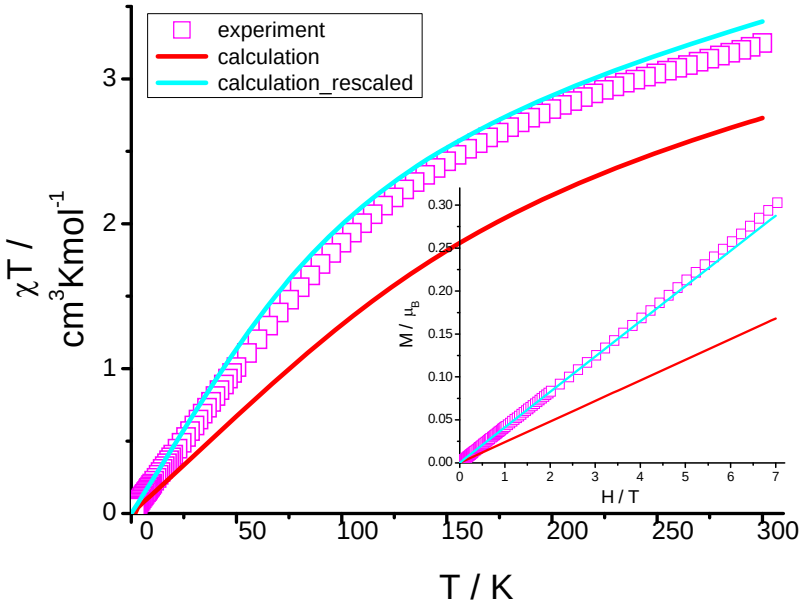

Figure S18: A comparison of the experimental and calculated (solid line) magnetic susceptibility and magnetization (inset) for **1** .The red curves are simulations corresponding to the basis set of column C from Table 4. The blue curves are the calculations for the modified energy of the first excited state (see the text).

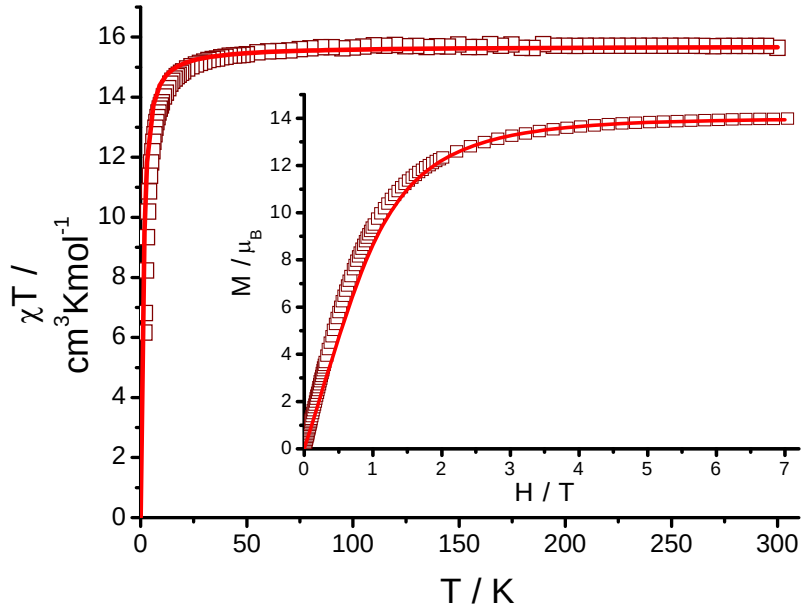

Figure S19: A comparison of the experimental and calculated (solid line) magnetic susceptibility and magnetization at 2K (inset) for **2**.

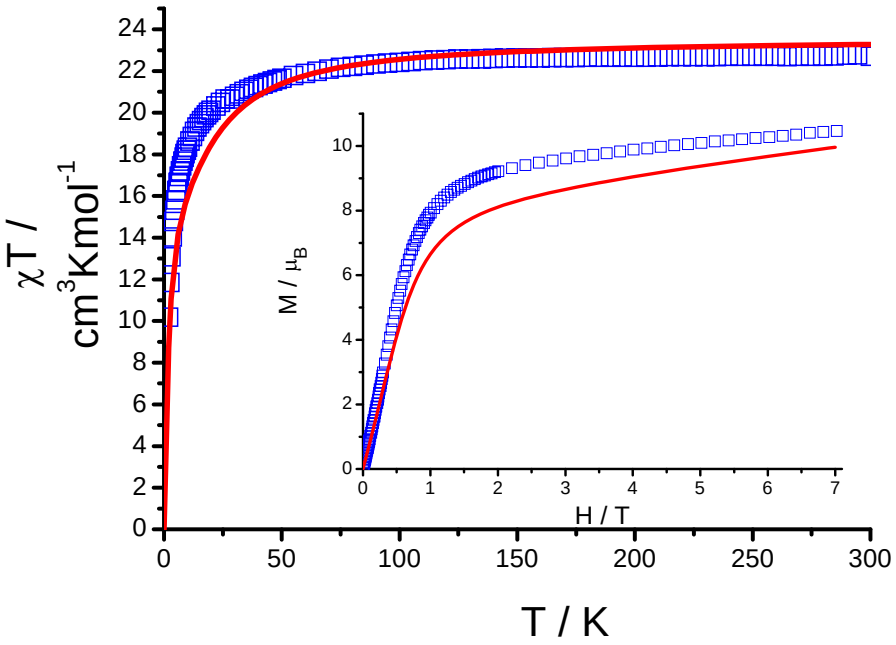

Figure S20: A comparison of the experimental and calculated (solid line) magnetic susceptibility and magnetization at 2K (inset) for **3**.

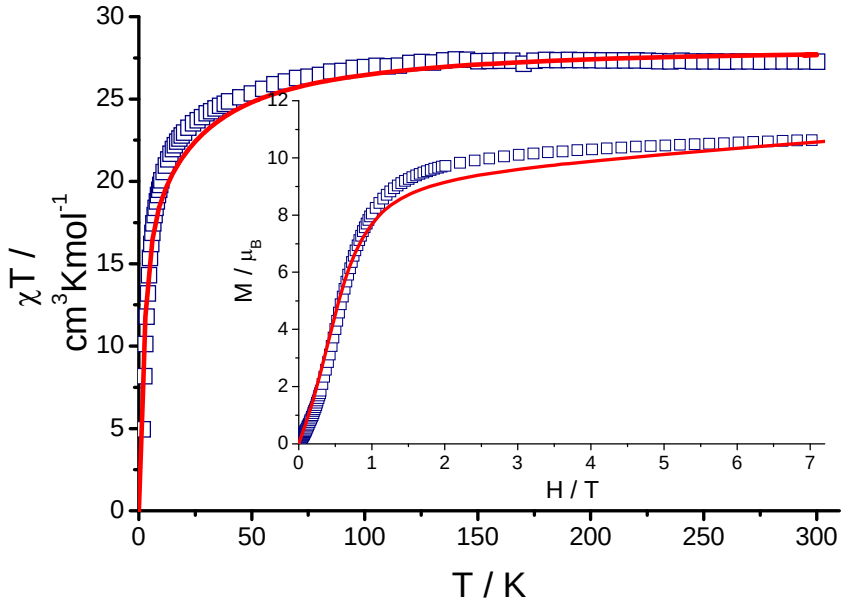

Figure S21: A comparison of the reduced by 8% experimental (empty squares) with the calculated (line) magnetic susceptibility and magnetization at 2K (inset) for **4**.

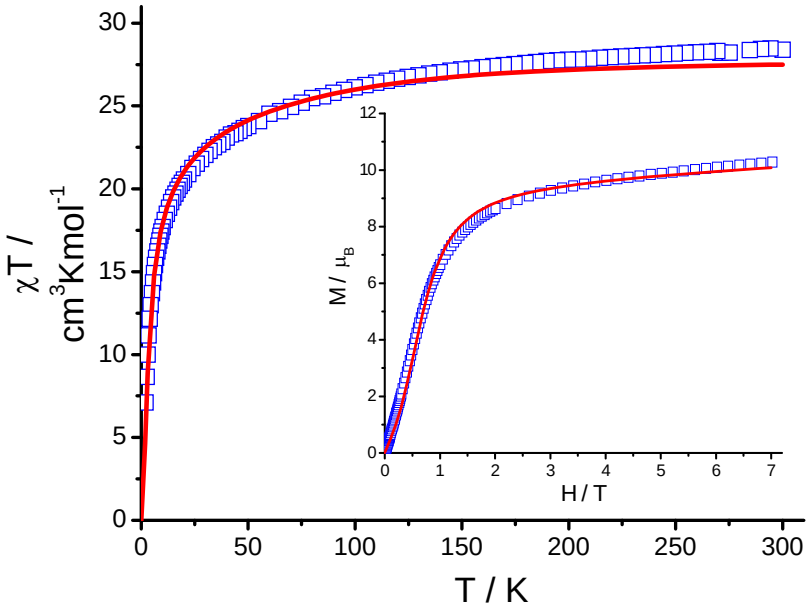

Figure S22: A comparison of the experimental and calculated (solid line) magnetic susceptibility and magnetization at 2K (inset) for **5**.